Doped Sr2FeIrO6 – phase separation and a Jeff ≠ 0 state for Ir5+

PAGE, Jacob, TOPPING, Craig, SCRIMSHIRE, Alex <http://orcid.org/0000-0002-6828-3620>, BINGHAM, Paul <http://orcid.org/0000-0001-6017-0798>, BLUNDELL, Stephen and HAYWARD, Michael

Citation:

Copyright and re-use policy

Doped Sr_2FeIrO_6 – phase separation and a $J_{eff} \neq 0$ state for Ir^{5+}

Jacob E. Page[†], Craig V. Topping[‡], Alex Scrimshire[Ψ], Paul A. Bingham[Ψ], Stephen J. Blundell[‡] and Michael A. Hayward [†]*.

† Department of Chemistry, University of Oxford, Inorganic Chemistry Laboratory, South Parks Road, Oxford, OX1 3QR, U.K.

‡ Department of Physics, Clarendon Laboratory, University of Oxford, Parks Road, Oxford, OX1 3PU, U.K.

Ψ Materials and Engineering Research Institute, Sheffield Hallam University, City Campus, Howard Street, Sheffield, S1 1WB, U.K.

ABSTRACT: High-resolution synchrotron X-ray and neutron powder diffraction data demonstrate that, in contrast to recent reports, Sr_2FeIrO_6 adopts an $I\bar{1}$ symmetry double perovskite structure with an $a^-b^-c^-$ tilting distortion. This distorted structure does not tolerate cation substitution, with low levels of A-site (Ca, Ba, La) or Fe-site (Ga) substitution leading to separation into two phases: a stoichiometric $I\bar{1}$ phase and a cation-substituted, $P2_1/n$ symmetry, $a^-a^-c^+$ distorted double perovskite phase. Magnetization, neutron diffraction and ^{57}Fe Mössbauer data show that in common with Sr_2FeIrO_6, the cation substituted $Sr_{2-x}A_xFe_{1-y}Ga_yIrO_6$ phases undergo transitions to type-II antiferromagnetically ordered states at $T_N \sim 120$ K. However, in contrast to stoichiometric Sr_2FeIrO_6, cation substituted samples exhibit a further magnetic transition at $T_A \sim 220$ K, which corresponds to the ordering of $r_{eff} \neq 0$ Ir^{5+} centers in the cation-substituted, $P2_1/n$ symmetry, double perovskite phases.

Introduction

There has been much interest recently in complex oxides containing 5d transition metals.[1] This is principally because the heavier members of the transition metal series exhibit strong spin-orbit coupling (SOC), which in many cases can be comparable in magnitude to on-site coulombic repulsions (U) or crystal field effects (Δ). As a result, when these interactions combine they can split the broad 5d manifold and localize the valence electrons in 5d transition-metal systems, despite the expectation that bands derived from 5d orbitals should be sufficiently broad to support itinerant electronic behavior under most conditions.

For example, in the case of octahedrally coordinated iridium centers, it is observed that the strong crystal field splits the 5d orbitals into the familiar e_g and t_{2g} sets, with the t_{2g} orbitals further split into quartet $J = \frac{3}{2}$ and doublet $J = \frac{1}{2}$ states under the influence of SOC. The $J = \frac{3}{2}$ state lies lower in energy, thus systems containing d^5, Ir^{4+} centers have a full $J = \frac{3}{2}$ band and a half filled $J = \frac{1}{2}$ band. This latter band is relatively narrow, so that modest coulombic repulsion energies can open a Mott gap, as seen for example in the insulating antiferromagnetic behavior of Sr_2IrO_4 [2] – a phase which might be expected to exhibit itinerant electronic behavior, based on the 4d analogue, Sr_2RhO_4, which is a metal.[3]

The similar magnitudes of the crystal field, coulombic and SOC interactions in 5d systems means that small adjustments to the balance between these terms can result in a wide variety of different electronic scenarios, and this has led to the predication of a host of exotic behaviors in systems where SOC effects play a significant role, hence the huge interest in complex oxides containing Ir^{4+} cations.[4-6]

Systems containing Ir^{5+} have received significantly less attention than the corresponding Ir^{4+} oxides. This is due in part to the initial impression that the electronic situation for $Ir^{5+}O_6$ centers is simpler than the Ir^{4+} case, as the d^4 electron count of $Ir^{5+}O_6$ centers is expected to lead to complete occupation of the $J = \frac{3}{2}$ state resulting in a local moment of $J_{eff} = 0$, and thus diamagnetic behavior.

Indeed many phases containing $Ir^{5+}O_6$ centers are observed to have very small moments.[7-8] However there are a number of studies which report non-zero moments for Ir^{5+} cations, which are not easily dismissed as being due to impurity phases.[9-12] The appearance of these $J_{eff} \neq 0$ states has been attributed to local distortions in the IrO_6 coordination weakening the SOC interaction,[13] or band structure effects arising from superexchange coupling.[14] Whatever the origin of the paramagnetism, these examples show that systems containing Ir^{5+} are not as simple as first imagined, and warrant further study.

$A_2BB'O_6$ double perovskite oxides which consist of ordered arrays of 3d (B) and 5d (B') transition-metal cations, offer an interesting framework in which to study SOC driven behaviors, because they can accommodate a wide variety of A, B and B' cations,[15] allowing less favored oxidation states, such as Ir^{5+}, to be stabilized. Furthermore, by combining the contrasting features of 3d metals (narrow 3d bands, large U, modest Δ, weak SOC) with 5d metals (wide 5d bands, modest U, strong Δ, strong SOC) and tuning their interactions via adjustment of the B-O-B' bond angles through A-cation substitution, it is possible to prepare phases with a wide variety of novel behavior. For example 3d-5d systems with itinerant electrons can exhibit spin-polarized conductivity and half-metallic behavior,[16-17] while in insulating systems magnetic
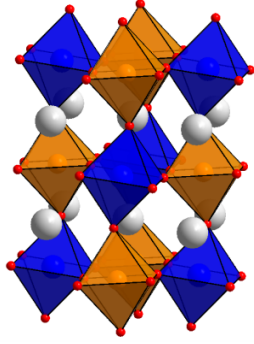
Figure 1. The crystal of Sr_2FeIrO_6. Grey, orange, blue and red spheres represent Sr, Fe, Ir and O respectively.

couplings which violate the Goodenough-Kanamori rules are observed,[18-19] with sequential magnetic ordering of the B' and B cation lattices observed in some cases.[20]

The double perovskite Sr_2FeIrO_6 (Figure 1) lies within this area of interest, as it contains arrays of Fe^{3+} and, nominally J_{eff} = 0, Ir^{5+} cations. However previous reports describing the crystallography and physical behavior of this phase are contradictory. Battle *et al.* first reported Sr_2FeIrO_6 as adopting an $I\bar{1}$ distorted ($a^-b^-c^-$ in Glazer notation[21-22]) double perovskite structure with ~7% Fe/Ir anti-site disorder.[23] [57]Fe Mossbauer data from this sample give a single sharp peak consistent with the highly symmetric $Fe^{3+}O_6$ units observed in the reported crystal structure. Battle *et al*, went on to report that on cooling below T_N ~ 120 K, Sr_2FeIrO_6 adopts a type II antiferromagnetically ordered magnetic structure, observed by neutron diffraction. In contrast an initial report by Bufaiçal *et al.* reported that Sr_2FeIrO_6 adopts an $P2_1/n$ ($a^-a^-c^+$) distorted double perovskite structure with ~16 % anti-site disorder.[24] [57]Fe Mossbauer data from this sample indicated there were two iron sites, a highly symmetric site analogous to that observed by Battle *et al.* and a less symmetric site. Close inspection of this sample revealed the presence of small amounts of Fe_2O_3. In a subsequent report Bufaiçal *et al.* described the preparation of a further sample of Sr_2FeIrO_6 by a different method.[25] This second sample was reported to adopt an $I2/m$ ($a^-a^-c^0$) distortion with ~6 % Fe/Ir anti-site disorder, however there was an indication that IrO_2 is present in this sample. Kayser *et al.* also report an $I2/m$ distorted structure with ~18% Fe/Ir anti-site disorder, although the magnetic data presented clearly indicate Fe_2O_3 is also present in the sample.[26] Qasim *et al.* also observe an $I2/m$ distortion for Sr_2FeIrO_6 but report "broadening of R-point super-lattice reflections" in their diffraction data.[27]

In combination these previous reports present a confused picture, and suggest the degree of Fe/Ir disorder and the tilting distortions adopted by Sr_2FeIrO_6 are sensitive to the synthesis conditions employed to prepare samples. We have therefore reinvestigated this phase and studied the influence of low levels of cation substitution on the structure and physical properties.

Experimental

Sample preparation. Samples of Sr_2FeIrO_6, $La_{0.025}Sr_{1.975}FeIrO_6$, $La_{0.05}Sr_{1.95}FeIrO_6$, $Ca_{0.05}Sr_{1.95}FeIrO_6$, $Ba_{0.0185}Ca_{0.0315}Sr_{1.95}FeIrO_6$ and $Sr_2Fe_{0.95}Ga_{0.05}IrO_6$ were prepared using a citrate gel method. Appropriate quantities of $SrCO_3$ (99.994%), La_2O_3 (99.99%, dried at 900°C), $CaCO_3$ (99.999%), $BaCO_3$ (99.997%), Ga_2O_3 (99.999%) and Fe (99.99%) were dissolved in a minimal quantity of a 1:1

Space Group	χ^2	wRp (%)	Rp (%)
$I\bar{1}$ (#2)	14.13	2.55	1.70
$I2/m$ (#12)	20.98	3.12	2.01
$P2_1/n$ (#14)	20.79	3.10	2.00

Table 1. Fitting statistics from the structural refinement of Sr_2FeIrO_6 against synchrotron X-ray powder diffraction data.

mixture of concentrated nitric acid and distilled water, then the required amount of IrO_2 (99.99%, dried at 700 °C for 2 hours) was added. Citric acid and analar ethylene glycol were added and the solution was heated whilst being stirred. The gel thus formed was allowed to combust in air and the subsequent product was ground into a fine powder, placed in an alumina crucible and heated at 1000 °C in air at a rate of 1 °C min^{-1}to remove the organic components of the sample. The resulting powder was pressed into a 13 mm diameter pellet and heated in air for two cycles of 2 days at 1100 °C.

Characterization. X-ray powder diffraction data were collected from using instrument I11 at the Diamond Light Source Ltd. From samples sealed inside 0.3 mm diameter borosilicate glass capillaries. Diffraction patterns were measured using Si-calibrated X-rays with and approximate wavelength 0.825 Å using the PSD detector. Neutron powder diffraction data were collected using the WISH instrument, at the ISIS neutron source, from samples contained within vanadium cans. Rietveld profile refinements were performed using the GSAS suite of programs.[28] Neutron diffraction data were corrected for strong Ir absorption prior to fitting, while analysis of synchrotron X-ray data utilized the Debye-Scherrer correction present in the GSAS suite. Magnetization data were collected using a Quantum Design MPMS SQUID magnetometer. Four-probe resistivity measurements were performed on bars cut from sintered pellets, using a Quantum design PPMS.

[57]Fe Mössbauer spectroscopy measurements utilized acrylic absorber discs with a sample area of 1.767 cm^2 which were loaded to present 2.16×10^{-3} g cm^{-2} of Fe, and achieve a Mössbauer thickness of 1. Samples were homogeneously mixed with graphite to achieve this level of loading. The 14.4 keV γ-rays were supplied by the cascade decay of 25 mCi [57]Co in a Rh matrix source, oscillated at constant acceleration by a SeeCo W304 drive unit, and detected using a SeeCo 45431 Kr proportional counter operating with 1.745 kV bias voltage applied to the cathode. All measurements were calibrated relative to α-Fe foil. Spectral data were fitted using the Recoil software package,[29] using Lorentzian line shapes. Sub-ambient temperatures were maintained using a Janis 10 K CCR cytostatic spectrometer (Model CCS-800/204N) and Lakeshore 335 temperature controller.

Characterization of Sr_2FeIrO_6. Models corresponding to the three different distorted double-perovskite frameworks previously reported for Sr_2FeIrO_6, in space groups $I\bar{1}$ (#2), $P2_1/n$ (#14) and $I2/m$ (#12),[23-25] were refined against synchrotron X-ray powder diffraction data collected from Sr_2FeIrO_6 at room temperature. During refinements the displacement parameters of atoms were constrained by type, but all other parameters were allowed to refine freely. Fitting statistics from these refinements (Table 1) indicate that the model in space group $I\bar{1}$ gives the best fit to the data. In addition inspection of fits to the data shown in Figure 2, confirm that the $I\bar{1}$ model accounts for the splitting of high index diffraction features more effectively than the other models. In combination these
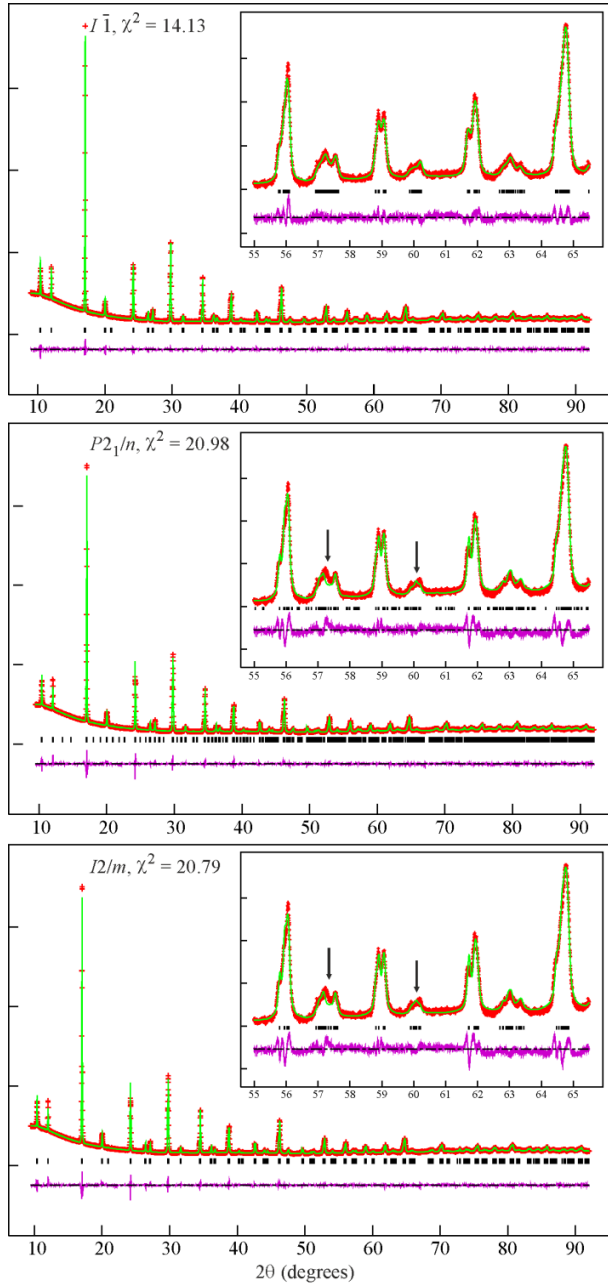
Figure 2. Observed, calculated and difference plots from the structural refinement of Sr_2FeIrO_6 against synchrotron X-ray powder diffraction data using models in space groups $I\bar{1}$ (top), $P2_1/n$ (middle) and $I2/m$ (bottom). Arrows indicate poorly fitted regions.

observations agree with the previous study by Battle *et al.* that Sr_2FeIrO_6 adopts an $I\bar{1}$ distorted double perovskite structure.[23] Close inspection of the diffraction data reveals no evidence for secondary phases (Fe_2O_3, IrO_2) suggesting that the sample has a 1:1 Fe:Ir elemental ratio. A complete description of the refined structure of Sr_2FeIrO_6 and selected bond lengths are given in Tables S1 and S2 the Supporting Information.

Magnetization-field isotherms collected from Sr_2FeIrO_6 at 300 K (Figure S3) are linear and pass through the origin, consistent with the absence of Fe_2O_3. Zero-field cooled (ZFC) and field cooled (FC) magnetization data collected from Sr_2FeIrO_6 (Figure 3) diverge at 120 K consistent with the onset of magnetic order, again in agreement with the report by Battle *et al*[23]

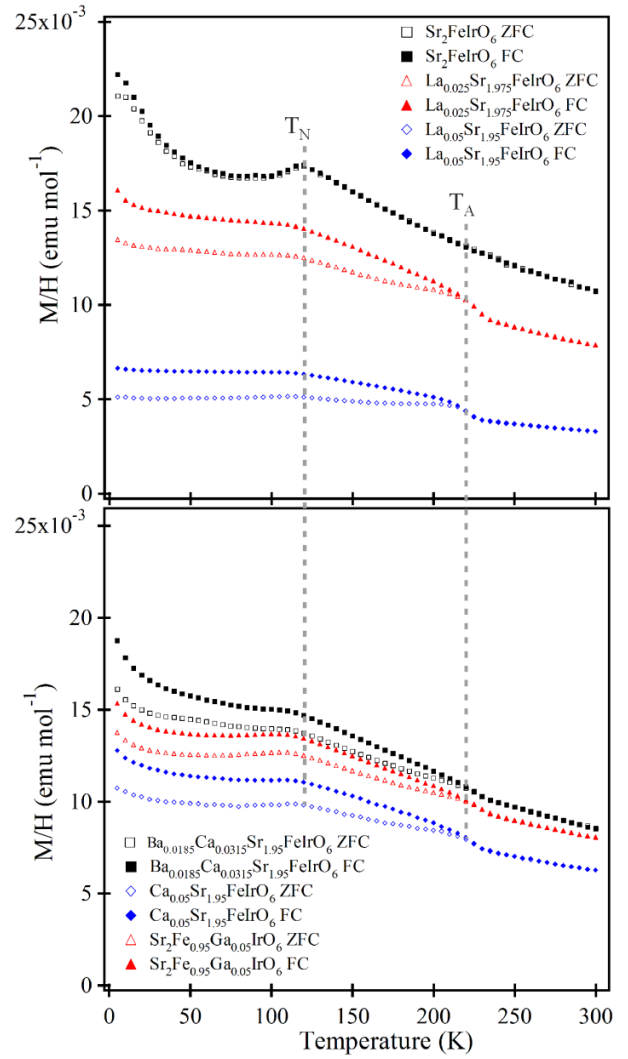**Figure 3. ZFC and FC magnetization data collected from cation substituted Sr_2FeIrO_6 samples in an applied field of 100 Oe.**

	Synchrotron X-ray			
Space Group	χ^2	wRp (%)	Rp (%)	Variables
$I\bar{1}$ (#2)	6.164	1.83	1.32	49
$I2/m$ (#12)	7.007	1.94	1.39	41
$P2_1/n$ (#14)	6.792	1.91	1.37	47
$I\bar{1}$+ $P2_1/n$	5.782	1.81	1.24	75
$I2/m$+$P2_1/n$	6.298	1.89	1.27	67
	Neutron			
Space Group	χ^2	wRp (%)	Rp (%)	Variables
$I\bar{1}$ (#2)	5.29	5.94	4.09	92
$I2/m$ (#12)	6.78	6.72	4.69	84
$P2_1/n$ (#14)	6.52	6.58	4.55	90
$I\bar{1}$+ $P2_1/n$	5.02	5.91	4.06	131
$I2/m$+$P2_1/n$	5.53	6.02	4.15	123

Table 2. Fitting statistics from the structural refinement of $La_{0.05}Sr_{1.95}FeIrO_6$ against synchrotron X-ray and neutron powder diffraction data.
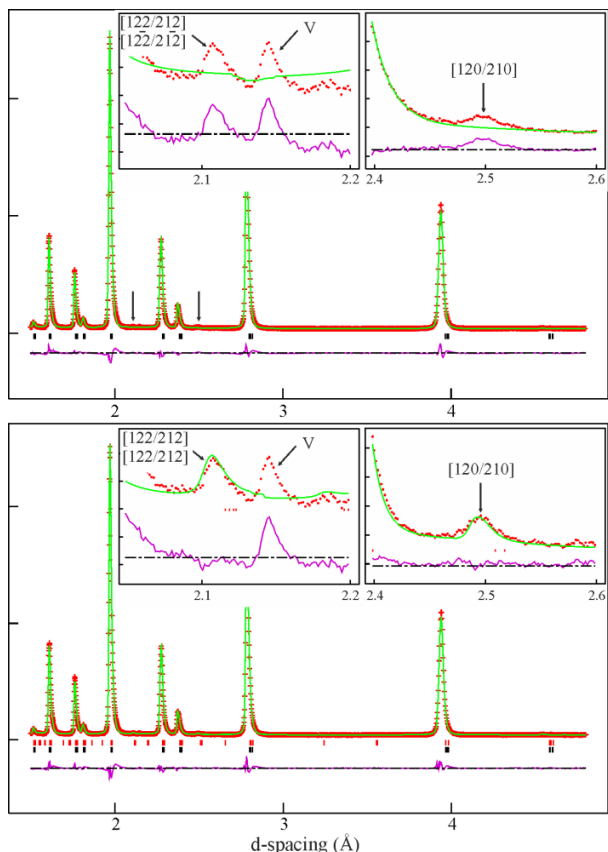
3

Figure 4. Observed, calculated and difference plots from the refinement of $La_{0.05}Sr_{1.95}FeIrO_6$ against neutron powder diffraction data (121° bank) collected at 250 K. (Top) refinement of an $I\bar{1}$ symmetry model. Additional peaks at d ~ 2.1 Å and 2.5 Å can only be indexed in a primitive unit cell. (Bottom) 2-phase refinement using models in space groups $I\bar{1}$ (bottom tick marks) and $P2_1/n$ (top tick marks).

Thus we can conclude that using the modified citrate synthesis method we can prepare stoichiometric samples of Sr_2FeIrO_6 comparable to the sample in the Battle *et al.* report.

Structural characterization of $La_{0.05}Sr_{1.95}FeIrO_6$. Following the procedure adopted for the undoped sample, the same 3 distorted double-perovskite structural models, in space groups $I\bar{1}$, $P2_1/n$ and $I2/m$, were refined against synchrotron X-ray powder diffraction data collected from $La_{0.05}Sr_{1.95}FeIrO_6$ at room temperature. In common with Sr_2FeIrO_6, the $I\bar{1}$ model gave the best fit to the synchrotron data (Table 2).

Likewise the $I\bar{1}$ model also gave the best fit to neutron powder diffraction data collected from $La_{0.05}Sr_{1.95}FeIrO_6$ at 250 K, however close inspection of the neutron diffraction data revealed a series of weak diffraction peaks which could only be indexed using a primitive unit cell, not a body-centered unit cell (Figure 4). In combination these observations suggested that the sample of $La_{0.05}Sr_{1.95}FeIrO_6$ was a mixture of 2 phases, one with an $I\bar{1}$ distorted structure and one with a $P2_1/n$ distorted structure. Thus a two-phase model utilizing both the $I\bar{1}$ and $P2_1/n$ models was refined against the synchrotron and neutron diffraction data to yield improved fits (Table 2). Neutron diffraction data from the 58°, 90°, 121°, 152° banks was utilized in the refinements. For completeness a further two-phase model consisting of a combination of $I2/m$ and $P2_1/n$ distorted double perovskite structures was also refined against the
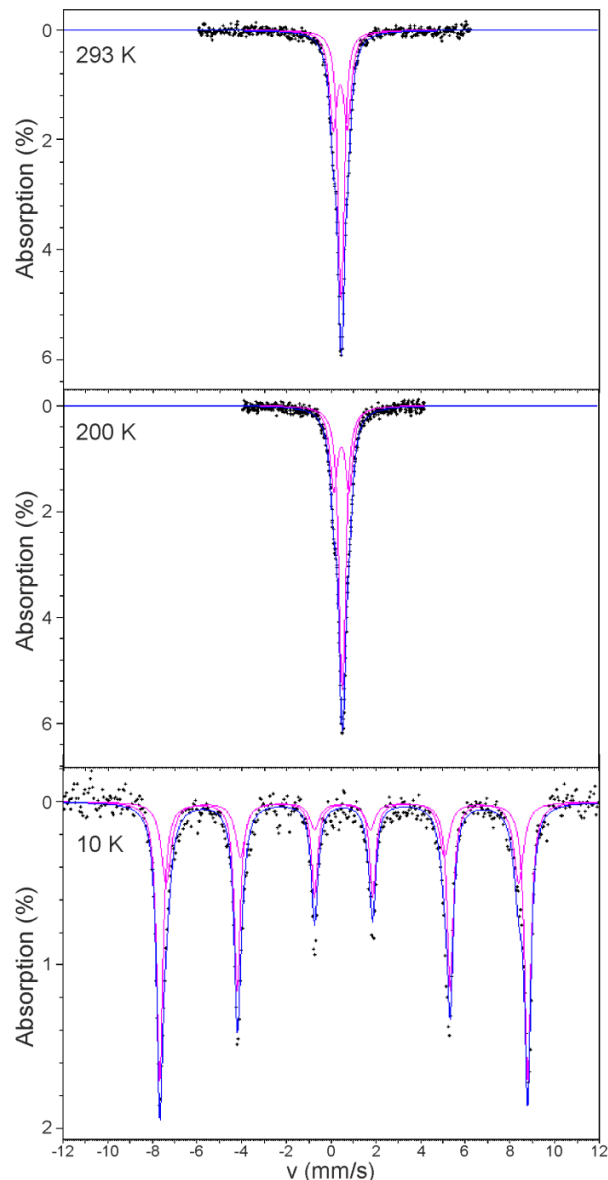

Figure 5. ^{57}Fe Mössbauer spectra collected from $La_{0.05}Sr_{1.95}FeIrO_6$ at 293 K, 200K, and 10 K. Fitting parameters are detailed in Table 4.

diffraction data, but this was observed to give a poorer fit than the $I\bar{1}$ + $P2_1/n$ combination (Table 2). Full details of the 2-phase model are given in Table S3, with selected bond lengths in Table S4 in the Supporting Information.

A ^{57}Fe Mössbauer spectrum collected from $La_{0.05}Sr_{1.95}FeIrO_6$ at room temperature (Figure 5) could be fitted to two signals, a sharp 'singlet', analogous to the spectrum observed by Battle *et al.* for Sr_2FeIrO_6,[23] and a broader

'doublet' consistent with a more distorted Fe^{3+} center (Table 4). We attribute the first sharp signal to the high-symmetry $Fe^{3+}O_6$ center in the $I\bar{1}$ phase and the 'doublet' to the more distorted $Fe^{3+}O_6$ units in the $P2_1/n$ symmetry phase. The relative areas of the two Mössbauer signals are approximately consistent with the relative fractions of the $I\bar{1}$ and $P2_1/n$ phases in the sample. We do not believe that the changes in the fractions as a function of temperature are significant, but rather arise from the difficulty in fitting broad, overlapping

I$\bar{1}$							
Sample	a(Å)	b(Å)	c(Å)	α(°)	β(°)	γ(°)	Fraction(%)
Sr_2	5.5519(2)	5.5779(2)	7.8445(2)	90.01(1)	90.04(1)	90.10(1)	100
$La_{0.05}Sr_{1.95}$	5.5497(1)	5.5781(1)	7.8463(1)	89.99(1)	90.06(1)	90.07(2)	44.3(9)
$La_{0.025}Sr_{1.975}$	5.552(1)	5.583(1)	7.847(1)	90.00(1)	90.08(1)	90.07(2)	76.2(9)
$Ca_{0.05}Sr_{1.95}$	5.556(1)	5.582(1)	7.846(1)	89.99(1)	90.06(1)	90.08(2)	53.5(9)
$Ba_{0.0185}Ca_{0.0315}Sr_{1.95}$	5.558(1)	5.589(1)	7.848(1)	89.99(1)	90.08(1)	90.08(2)	53.8(8)
$Fe_{0.95}Ga_{0.05}$	5.557(1)	5.586(1)	7.849(1)	89.98(1)	90.08(1)	90.09(2)	69.4(9)

$P2_1/n$					
Sample	a(Å)	b(Å)	c(Å)	β(°)	Fraction(%)
$La_{0.05}Sr_{1.95}$	5.5515(1)	5.5810(1)	7.8462(1)	90.08(1)	55.7(9)
$La_{0.025}Sr_{1.975}$	5.564(1)	5.583(1)	7.848(1)	90.07(1)	23.8(9)
$Ca_{0.05}Sr_{1.95}$	5.556(1)	5.585(1)	7.849(1)	90.09(1)	46.5(9)
$Ba_{0.0185}Ca_{0.0315}Sr_{1.95}$	5.581(1)	5.592(1)	7.857(1)	90.04(1)	46.2(8)
$Fe_{0.95}Ga_{0.05}$	5.561(1)	5.580(1)	7.857(1)	90.06(1)	30.6(9)

Table 3. Lattice parameters from the 2-phase refinements of cation substituted Sr_2FeIrO_6

T (K)	Site 1					Site 2					χ^2
	CS (mm/s)	Δ (mm/s)	B_{hf} (T)	HWHM (mm/s)	%	CS (mm/s)	Δ (mm/s)	B_{hf} (T)	HWHM (mm/s)	%	
293	0.400(6)	0.634(3)	0	0.205(1)	47.0(6)	0.437(2)	0.115(1)	0	0.134(2)	53.0(6)	0.595
200	0.459(5)	0.691(2)	0	0.201(1)	39.9(5)	0.496(1)	0.122(1)	0	0.148(2)	60.1(5)	0.572
10	0.507(22)	-	48.90(3)	0.265(5)	31(8)	0.563(2)	-	51.05(5)	0.164(1)	68(7)	0.709

Table 4. Parameters extracted from fits to ^{57}Fe Mössbauer spectra collected from $La_{0.05}Sr_{1.95}FeIrO_6$

features. We note that this spectrum is qualitatively very similar to the ^{57}Fe Mössbauer spectrum collected by Bufaiçal *et al.* from their sample of Sr_2FeIrO_6.[24]

Magnetic and Low-temperature structural characterization of $La_{0.05}Sr_{1.95}FeIrO_6$. ZFC and FC magnetization data collected from $La_{0.05}Sr_{1.95}FeIrO_6$ (Figure 3) show an additional magnetic transition compared to the equivalent data collected from Sr_2FeIrO_6, with the data sets diverging below T ~ 220 K (henceforth referred to as T_A) before going through a localmaximum at 120 K (T_N) which corresponds to the reported magnetic ordering temperature of Sr_2FeIrO_6.[23]

An ^{57}Fe Mössbauer spectrum collected from $La_{0.05}Sr_{1.95}FeIrO_6$ at 10 K, shown in Figure 5, can be fitted to two magnetic sextets (Table 4) indicating that both the $I\bar{1}$ and $P2_1/n$ phases are magnetically ordered. Neutron powder diffraction data collected from $La_{0.05}Sr_{1.95}FeIrO_6$ at 1.5 K exhibit additional diffraction features, compared to equivalent data collected at 250 K, which can be indexed as a $1 \times 2 \times 2$ geometric expansion of either the $I\bar{1}$ or $P2_1/n$ crystallographic cells (Supporting Information). The observed intensities of the additional reflections can be accounted for using the type II antiferromagnetic model, shown in Figure 6, reported for Sr_2FeIrO_6. It was not possible to refine individual magnetic models for the $I\bar{1}$ and $P2_1/n$ phases, instead a single magnetic model was used to account for the magnetic scattering from both crystallographic phases, as described in the supporting information, yielding an ordered moment of 2.92(2) μ_B per Fe center. On warming from 1.5 K the magnetic diffraction features in the neutron diffraction data weaken, becoming undetectable at temperatures above 120 K (T_N), with the observed diffraction data above this temperature being accounted for by nuclear scattering
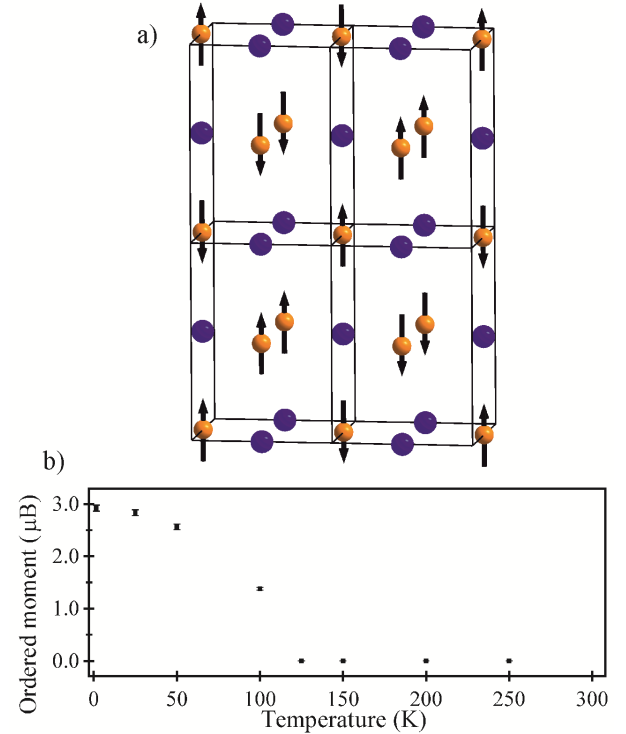

Figure 6. a) The type-II antiferromagnetic structure of $La_{0.05}Sr_{1.95}FeIrO_6$. Blue and orange spheres represent Ir and Fe respectively. b) The ordered moment per Fe center as a function of temperature.

5

alone, thus there does not appear to be any magnetic scattering associated with the magnetization anomaly at 210 K (T_A). A plot of the ordered magnetic moment as a function of temperature is shown in Figure 6. A ^{57}Fe Mössbauer spectrum collected from La$_{0.05}$Sr$_{1.95}$FeIrO$_6$ at 200 K is very similar to the equivalent spectrum collected at 293 K (Figure 5) and can be fitted to the same combination of a sharp singlet and broad doublet as the high temperature spectrum, with no indication of magnetically ordered iron centers.

The non-magnetic scattering features in the low-temperature neutron diffraction data collected from La$_{0.05}$Sr$_{1.95}$FeIrO$_6$ can be accounted for using the same 2-phase model which was fitted to the equivalent data collected at 250 K. Refinement of the phase fractions reveal that these do not change within error, as a function of temperature, as detailed in Table S7 in the supporting information.

To further characterize the temperature-dependent behavior of La$_{0.05}$Sr$_{1.95}$FeIrO$_6$ a series of synchrotron X-ray powder diffraction patterns were collected with intervals of approximately 1.5 K, over the temperature range 100 < T/K < 300. These data were fitted to the same two phase model ($I\bar{1}$ + $P2_1/n$) utilized for the neutron diffraction data. The lattice parameters of the $I\bar{1}$ phase show no strong anomalies at T_A (Figure S9). In contrast the a lattice parameter of the $P2_1/n$ phase shows a distinct local maximum at T_A = 220 K (Figure 7) while b shows a change in expansion rate, consistent with the onset of magnetic order in the monoclinic phase, which is responsible for divergence in the magnetization data.

Transport data. Resistivity data collected from Sr$_2$FeIrO$_6$ and La$_{0.05}$Sr$_{1.95}$FeIrO$_6$ (Figure 8) indicate that both samples are highly resistive. Both data sets exhibit a local maximum at T ~ 100 K coincident with the onset of antiferromagnetic order (T_N), but there is no feature in the La$_{0.05}$Sr$_{1.95}$FeIrO$_6$ data at T_A. Plots of the data to investigate Arrhenius behavior (ln ρ vs 1/T) or variable range hopping behavior (ln ρ vs T$^{-1/4}$) did not give convincing linear behavior over any significant temperature range, as shown in the supporting information. It should be noted that as these measurements were performed on compressed powder samples it is not possible to disentangle intrinsic and grain-boundary effects.

Structural and magnetic characterization of other cation substituted Sr$_2$FeIrO$_6$ phases. Following the procedure described above for La$_{0.05}$Sr$_{1.95}$FeIrO$_6$, the same 5 structural models were refined against synchrotron X-ray powder diffraction data collected from La$_{0.025}$Sr$_{1.975}$FeIrO$_6$, Sr$_{1.95}$Ca$_{0.05}$FeIrO$_6$, Ba$_{0.0185}$Ca$_{0.0315}$Sr$_{1.95}$FeIrO$_6$ and Sr$_2$Fe$_{0.95}$Ga$_{0.05}$IrO$_6$. For all samples it was observed that the $I\bar{1}$ model gave the best single-phase fit, but that in all cases a 2-phase model consisting of a combination of $I\bar{1}$ and $P2_1/n$ symmetry phases was superior as shown in Tables S7-S10 in the Supporting Information. Lattice parameters and phase fractions extracted from these 2-phase refinements are listed in Table 3. Close inspection of the diffraction data revealed no evidence for secondary phases (Fe$_2$O$_3$, IrO$_2$). In addition magnetization-field data collected from samples at 300 K (Figures S4-S8) are linear and pass through the origin, confirming that no Fe$_2$O$_3$ is present in the samples.

Magnetization data collected from these cation substituted phase (Figure 3) are qualitatively similar to those of La$_{0.05}$Sr$_{1.95}$FeIrO$_6$ exhibiting a divergence between ZFC and FC data at T_A ~ 220 K and a further local maximum at T_N ~ 120 K.
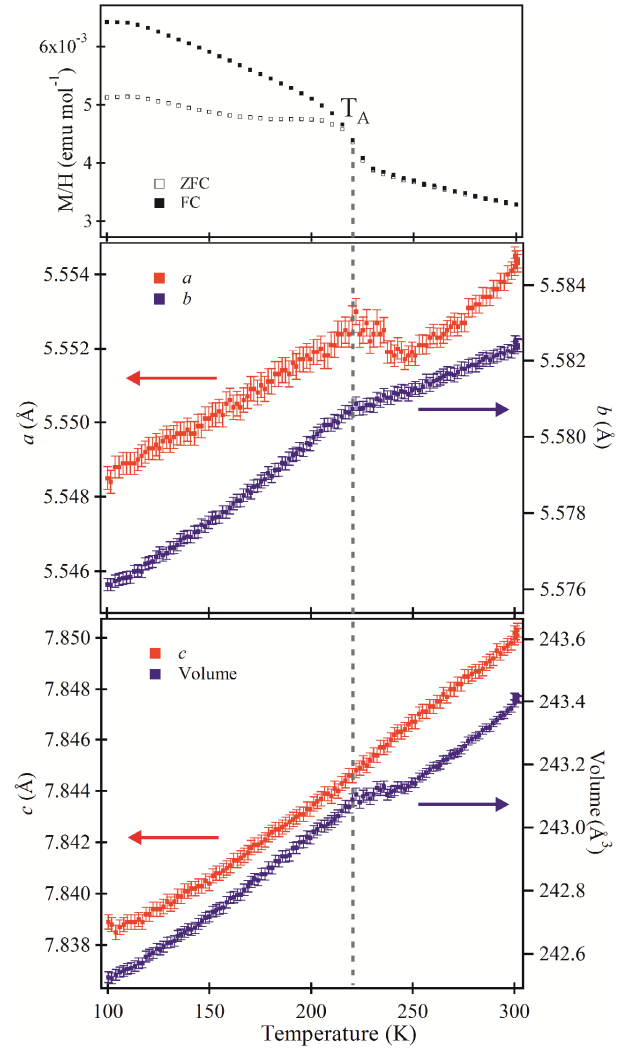

Figure 7. Magnetization data (top) and lattice parameters and cell volume of $P2_1/n$ phase (middle, bottom) of La$_{0.05}$Sr$_{1.95}$FeIrO$_6$ plotted as a function of temperature. Plotted lines are guides to the eye.
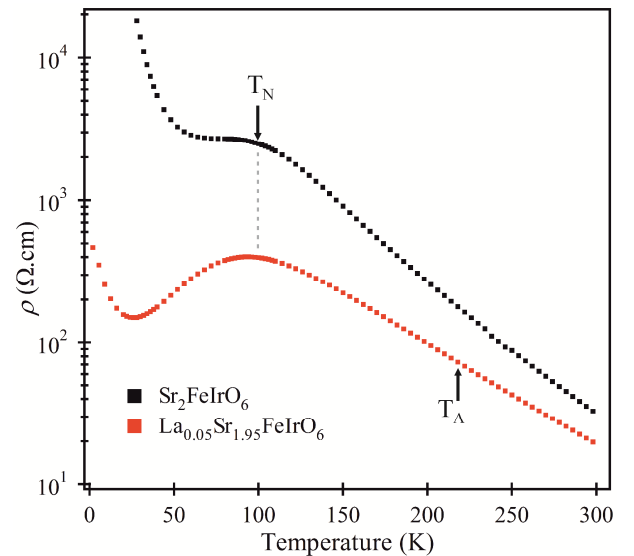

Figure 8. Temperature dependent resistivity data collected from Sr$_2$FeIrO$_6$ and La$_{0.05}$Sr$_{1.95}$FeIrO$_6$ on warming.

6

Discussion

Phase separation. Diffraction data show that Sr_2FeIrO_6, prepared *via* a modified citrate method, adopts an $I\bar{1}$ distorted double perovskite structure. However all the cation-substituted phases prepared by the same method separate into mixtures of $I\bar{1}$ and $P2_1/n$ distorted structures. Data extracted from the 2-phase refinements of the cation substituted phases (Table 3) show that the lattice parameters of the $I\bar{1}$ phases in different samples are remarkably similar to each other and to those of stoichiometric Sr_2FeIrO_6. In contrast, there is a wider variation in the lattice parameters of the $P2_1/n$ phases. This suggests that the cation substituted samples consist of a stoichiometric, $I\bar{1}$ symmetry Sr_2FeIrO_6 phase and a cation substituted phase with $P2_1/n$ symmetry, an idea further supported by the observation that the mass fraction of the $P2_1/n$ phase in the $La_{0.05}Sr_{1.95}FeIrO_6$ sample is approximately twice that in the $La_{0.025}Sr_{1.975}FeIrO_6$ sample (Table 3). Further heating of samples at 1100 ºC did not change the relative phase fractions of the $I\bar{1}$ and $P2_1/n$ phases within samples, nor did it lead to the formation of secondary phases (Fe_2O_3, IrO_2) , indicating that the observed phase separation is not due to incomplete reaction. Furthermore, variable temperature diffraction data indicate that the relative fraction of the $I\bar{1}$ and $P2_1/n$ phases in $La_{0.05}Sr_{1.95}FeIrO_6$ do not change as a function of temperature, reinforcing the idea that this is a chemical phase separation.

Given the wide variety of substituent cations used (La^{3+}, Ca^{2+}, Ba^{2+}, Ga^{3+}) we have made aliovalent (La^{3+}) and isovalent (Ca^{2+}, Ba^{2+}) A-site substitutions; we have made substitutions which lower the structural tolerance factor (La^{3+}, Ca^{2+}) and substitutions which maintain it (Ca^{2+}/Ba^{2+}) and we have also made isovalent substitutions on the B-site (Ga^{3+}). All of these cation substitutions led to phase separation suggesting that the $I\bar{1}$ distortion is only stable for stoichiometric Sr_2FeIrO_6 and that none of these cations have significant solubility in $I\bar{1}$ Sr_2FeIrO_6. This lack of solubility is surprising, however one explanation for this comes from the observation that the $I\bar{1}$ symmetry phase of Sr_2FeIrO_6 has a significantly lower degree of Fe/Ir antisite disorder than the $P2_1/n$ phases, suggesting that the $I\bar{1}$ structure is stabilized by high levels of Fe/Ir B-site order.

Studies of the B-site cation order of double perovskite oxides indicate that cation order is favored by a large difference in charge and/or size between cations, with charge being the more important factor.[15, 30-31] Surveys of known double perovskite oxides lead to the general conclusion that a charge difference of 3 units or greater will almost certainly lead to cation-ordered phases, while smaller charge differences can lead to ordered or disordered structures being preferred. The two-unit charge difference between the Fe^{3+} and Ir^{5+} ions in Sr_2FeIrO_6 suggests that the thermodynamic favorability of high levels of cation order is marginal for this compound, but that cation order is stabilized by the $I\bar{1}$ distortion. Following this reasoning we can see that small compositional changes, such as the B-site substitution of Ga for Fe, which add disorder to the Fe lattice and thus perturb the Fe/Ir cation order, will destabilize the $I\bar{1}$ structure, driving the system to separate into a stoichiometric $I\bar{1}$ Sr_2FeIrO_6 fraction and a gallium-containing $P2_1/n$ fraction, as observed. Similarly we propose that the size-disorder introduced on substitution of Sr on the A-site is also enough to destabilize the cation-ordered $I\bar{1}$ phase, again leading to a separation into a stoichiometric, $I\bar{1}$ symmetry, Sr_2FeIrO_6 fraction and an A-site substituted, $P2_1/n$ fraction.

This high structural sensitivity to the precise stoichiometry of samples also provides an explanation for the contradictory reports of the structure of Sr_2FeIrO_6. As noted above, iridium oxides can be volatilized when heated in the presence of oxygen. Thus iron-rich $Sr_2Fe_{1+x}Ir_{1-x}O_6$ samples can easily be prepared unintentionally if steps are not taken to avoid iridium loss. Our data indicates that the resulting non-stoichiometric samples would phase separate into complex mixtures of $I\bar{1}$ and $P2_1/n$ phases which are difficult to accurately analyze in the absence of high resolution diffraction data, leading to the reports of Sr_2FeIrO_6 adopting $P2_1/n$ and $I2/m$ distortions.

Magnetic behavior. The magnetic behavior of cation-substituted Sr_2FeIrO_6 is striking. Focusing on $La_{0.05}Sr_{1.95}FeIrO_6$ as an example, [57]Fe Mossbauer and neutron powder diffraction data show that the iron lattice of both the $I\bar{1}$ and $P2_1/n$ phases of this sample are ordered into type II antiferromagnetic lattices below $T_N \sim 120$ K. In addition magnetization data show a further anomaly at $T_A \sim 220$ K which coincides with anomalies in the lattice parameters of the $P2_1/n$ phase. [57]Fe Mossbauer data collected at 200 K (i.e. below T_A but above T) show no indication of any iron-based magnetic order, which leads us to conclude that the divergence between ZFC and FC magnetization data observed at 220 K is due to the ordering of iridium based spins within the $P2_1/n$ phase of the sample. The lack of any signature of magnetic order in the neutron diffraction data in the interval $T_N < T < T_A$ indicates that the ordered iridium moment is very small.

A simple explanation for the T_A magnetic anomaly in the lanthanum-substituted samples is that it is due to the presence of Ir^{4+} formed by the aliovalent La-for-Sr cation substitution. However this explanation does not stand up to scrutiny for a number of reasons. Firstly the concentration of Ir^{4+} will be very low in the $La_xSr_{2-x}FeIrO_6$ samples (<10%) so there will be a large spatial separation between Ir^{4+} centers, and it is hard to see how such a dilute lattice could order and cause a divergence between ZFC and FC magnetization data at T_A. Secondly, the same magnetic anomaly is observed in systems with isovalent cation substitutions (Ca, Ba, Ga) suggesting this is a bulk effect intrinsic to the $P2_1/n$ phases and not induced by low levels of Ir^{4+}.

As noted above, spin-orbit coupling is expected to act on octahedrally coordinated Ir^{5+} cations to yield $J_{eff} = 0$ ground states, a feature which appears to be at odds with our tentative assignment that the anomaly at T_A is due to the magnetic ordering of Ir^{5+} cations. However, reports describing double perovskite oxides containing Ir^{5+} centers almost always report non-zero iridium moments. For example Ba_2ScIrO_6 and Sr_2ScIrO_6 are observed to have moments of 0.16 and 0.39 μ_B/Ir respectively,[7] while $LaSrMgIrO_6$ and $LaSrZnIrO_6$ have moments of 0.61 and 0.46 μ_B/Ir respectively.[8] These magnetic responses are generally attributed to 'magnetic impurities' such as the presence of small quantities (1-2%) of Ir^{6+} or Ir^{4+} in samples due to non-stoichiometry or cation disorder.

Despite the general attribution of paramagnetic behavior in Ir^{5+} systems to low levels of Ir^{4+} or Ir^{6+}, there are reports of paramagnetic behavior in Ir^{5+} systems which are harder to simply dismiss as being due to impurities. For example single crystals of the double perovskite Sr_2YIrO_6 are observed to have local moments ranging between 0.91 and 0.21 μ_B/Ir with evidence in magnetization and heat capacity data for long range magnetic order below 1.4 K in one sample.[9-10] Similarly, single crystals of Ba_2YIrO_6 have been observed to have local

7

moments ranging between 0.62 and 0.42 μ_B/Ir, again with evidence for magnetic order below 1.7 K in one sample.[11-12]

This paramagnetic behavior of A_2YIrO_6 phases was initially attributed to a distortion of the IrO_6 units from strict O_h symmetry weakening the SOC and leading to $J_{eff} \neq 0$ behavior via an excitonic mechanism.[9, 13] However subsequent calculations indicated that the observed distortion of the IrO_6 octahedra is insufficient for the crystal field to quench the spin-orbit coupling, and instead ascribe the non-zero moments of iridium to band structure effects and super-exchange coupling between Ir centers,[14] although further studies have suggested even these interactions are not sufficient to stabilize paramagnetic states.[32]

Currently these studies of paramagnetic behavior in Ir^{5+} systems paint a rather unclear picture, with the mechanism for stabilizing $J_{eff} \neq 0$ states, and even their existence, still a matter of debate. However they do suggest a possible scenario in which paramagnetic Ir^{5+} states could be stabilized in the $P2_1/n$ phases of cation substituted Sr_2FeIrO_6.

As noted in Table S4, neutron diffraction data show that the $Ir^{5+}O_6$ units in the $P2_1/n$ phase of $La_{0.05}Sr_{1.95}FeIrO_6$ are more distorted that the equivalent, highly symmetric units in stoichiometric, $I\bar{1}$ Sr_2FeIrO_6. This decrease in $Ir^{5+}O_6$ symmetry is corroborated by the ^{57}Fe Mossbauer data which show the corresponding FeO_6 units are also considerably more distorted in the $P2_1/n$ phase. This increased level of MO_6 distortion, potentially in combination with Ir-O...O-Ir super-superexchange and Ir-O-Fe-O-Ir super-exchange coupling, could act to stabilize a $J_{eff} \neq 0$ state for the Ir^{5+} centers. The magnetic anomaly at 220 K can then be explained by the ordering of these paramagnetic Ir^{5+} centers, followed by the ordering of the Fe^{3+} centers on cooling below 120 K, in an analogy to the sequential ordering of Os^{6+} and Co^{2+} centers in Sr_2CoOsO_6.[20] The relatively high magnetic ordering temperature for the Ir^{5+} centers in cation-substituted Sr_2FeIrO_6 (220K) compared to those observed for A_2YIrO_6 phases (< 2K) can be rationalized by the presence of a non-d^0 transition metal cation (Fe^{3+}) on the B-cation site, as a similar strengthening of magnetic couplings on the introduction of a 3d transition-metal has been observed in osmium double perovskite phases.[33]

We note that the magnitude of the magnetic anomaly at T_A (a divergence between ZFC and FC data of $\sim 2 \times 10^{-3}$ emu mol^{-1} at 150 K) is sufficiently small that it would not be observed in previously reported samples, where the presence of Fe_2O_3 or other impurities mean that the ZFC/FC data divergence is significantly greater than this value at 220 K.

Conclusions

The volatility of iridium under conditions typically used to prepare complex oxides makes the synthesis of stoichiometric, iridium-containing, oxide double-perovskite phases challenging. This is particularly apparent for Sr_2FeIrO_6, where the ground state $I\bar{1}$ symmetry, double-perovskite structure is very sensitive to any deviations in stoichiometry, either through intentional doping or unintentional iridium loss, phase separating into a stoichiometric $I\bar{1}$ phase and a non-stoichiometric, $P2_1/n$ symmetry phase.

Magnetization data indicate that the Ir^{5+} centers in the doped $P2_1/n$ phases are good candidates for $J_{eff} \neq 0$ behavior, although the mechanism by which this unusual paramagnetic state is stabilized is yet to be established. It is clear this system warrants further attention.

AUTHOR INFORMATION

Corresponding Author

michael.hayward@chem.ox.ac.uk

Author Contributions

The manuscript was written through contributions of all authors. The authors declare no competing financial interests.

REFERENCES

1. Cao, G.; DeLong, L., *Frontiers of 4d- and 5d- Transition Metal Oxides*. World Scientific Publ Co Pte Ltd: Singapore, 2013; p 1-319.
2. Cao, G.; Bolivar, J.; McCall, S.; Crow, J. E.; Guertin, R. P., Weak ferromagnetism, metal-to-nonmetal transition, and negative differential resistivity in single-crystal Sr_2IrO_4. *Phys. Rev. B* **1998**, *57*, R11039-R11042.
3. Perry, R. S.; Baumberger, F.; Balicas, L.; Kikugawa, N.; Ingle, N. J. C.; Rost, A.; Mercure, J. F.; Maeno, Y.; Shen, Z. X.; Mackenzie, A. P., Sr_2RhO_4: a new, clean correlated electron metal. *New J. Phys.* **2006**, *8*, 14.
4. Jackeli, G.; Khaliullin, G., Mott Insulators in the Strong Spin-Orbit Coupling Limit: From Heisenberg to a Quantum Compass and Kitaev Models. *Phys. Rev. Lett.* **2009**, *102*.
5. Wang, F.; Senthil, T., Twisted Hubbard Model for Sr_2IrO_4: Magnetism and Possible High Temperature Superconductivity. *Phys. Rev. Lett.* **2011**, *106*.
6. Yang, K. Y.; Lu, Y. M.; Ran, Y., Quantum Hall effects in a Weyl semimetal: Possible application in pyrochlore iridates. *Phys. Rev. B* **2011**, *84*.
7. Kayser, P.; Kennedy, B. J.; Ranjbar, B.; Kimpton, J. A.; Avdeev, M., Spin-Orbit Coupling Controlled Ground State in the Ir(V) Perovskites A_2ScIrO_6 (A = Ba or Sr). *Inorg. Chem.* **2017**, *56*, 2204-2209.
8. Wolff, K. K.; Agrestini, S.; Tanaka, A.; Jansen, M.; Tjeng, L. H., Comparative Study of Potentially J(eff)=0 Ground State Iridium(V) in $SrLaNiIrO_6$, $SrLaMgIrO_6$, and $SrLaZnIrO_6$. *Z. Anorg. Allg. Chem.* **2017**, *643*, 2095-2101.
9. Cao, G.; Qi, T. F.; Li, L.; Terzic, J.; Yuan, S. J.; DeLong, L. E.; Murthy, G.; Kaul, R. K., Novel Magnetism of $Ir^{5+}(5d(4))$ ions in the Double Perovskite Sr_2YIrO_6. *Phys. Rev. Lett.* **2014**, *112*.
10. Corredor, L. T.; Aslan-Cansever, G.; Sturza, M.; Manna, K.; Maljuk, A.; Gass, S.; Dey, T.; Wolter, A. U. B.; Kataeva, O.; Zimmermann, A.; Geyer, M.; Blum, C. G. F.; Wurmehl, S.; Buchner, B., Iridium double perovskite Sr_2YIrO_6: A combined structural and specific heat study. *Phys. Rev. B* **2017**, *95*.
11. Dey, T.; Maljuk, A.; Efremov, D. V.; Kataeva, O.; Gass, S.; Blum, C. G. F.; Steckel, F.; Gruner, D.; Ritschel, T.; Wolter, A. U. B.;

Geck, J.; Hess, C.; Koepernik, K.; van den Brink, J.; Wurmehl, S.; Buchner, B., Ba_2YIrO_6: A cubic double perovskite material with Ir^{5+} ions. *Phys. Rev. B* **2016**, *93*.

12. Terzic, J.; Zheng, H.; Ye, F.; Zhao, H. D.; Schlottmann, P.; De Long, L. E.; Yuan, S. J.; Cao, G., Evidence for a low-temperature magnetic ground state in double-perovskite iridates with $Ir^{5+}(5d(4))$ ions. *Phys. Rev. B* **2017**, *96*.

13. Khaliullin, G., Excitonic Magnetism in Van Vleck-type d(4) Mott Insulators. *Phys. Rev. Lett.* **2013**, *111*.

14. Bhowal, S.; Baidya, S.; Dasgupta, I.; Saha-Dasgupta, T., Breakdown of J=0 nonmagnetic state in d(4) iridate double perovskites: A first-principles study. *Phys. Rev. B* **2015**, *92*, 5.

15. Vasala, S.; Karppinen, M., $A_2B'B''O_6$ perovskites: a review. *Prog. Solid St. Chem.* **2015**, *43*, 1-36.

16. Kobayashi, K. I.; Kimura, T.; Tomioka, Y.; Sawada, H.; Terakura, K.; Tokura, Y., Intergrain tunneling magnetoresistance in polycrystals of the ordered double perovskite Sr_2FeReO_6. *Phys. Rev. B* **1999**, *59*, 11159-11162.

17. Kato, H.; Okuda, T.; Okimoto, Y.; Tomioka, Y.; Takenoya, Y.; Ohkubo, A.; Kawasaki, M.; Tokura, Y., Metallic ordered double-perovskite Sr_2CrReO_6 with maximal Curie temperature of 635 K. *Appl. Phys. Lett.* **2002**, *81*, 328-330.

18. Kanungo, S.; Yan, B. H.; Jansen, M.; Felser, C., Ab initio study of low-temperature magnetic properties of double perovskite Sr_2FeOsO_6. *Phys. Rev. B* **2014**, *89*, 214414.

19. Ou, X. D.; Li, Z. W.; Fan, F. R.; Wang, H. B.; Wu, H., Long-range magnetic interaction and frustration in double perovskites Sr_2NiIrO_6 and Sr_2ZnIrO_6. *Scientific Reports* **2014**, *4*, 7542:1-4.

20. Morrow, R.; Mishra, R.; Restrepo, O. D.; Ball, M. R.; Windl, W.; Wurmehl, S.; Stockert, U.; Buchner, B.; Woodward, P. M., Independent ordering of two interpenetrating magnetic sublattices in the double perovskite Sr_2CoOsO_6. *J. Am. Chem. Soc.* **2013**, *135*, 18824-18830.

21. Glazer, A. M., Classification of tilted Octahedra in Perovskites. *Acta Crystallogr. Sect. B-Struct. Commun.* **1972**, *B 28*, 3384-3392.

22. Woodward, P. M., Octahedral tilting in perovskites .1. Geometrical considerations. *Acta Crystallogr. Sect. B-Struct. Commun.* **1997**, *53*, 32-43.

23. Battle, P. D.; Blake, G. R.; Gibb, T. C.; Vente, J. F., Structural chemistry and electronic properties of Sr_2FeIrO_6. *J. Solid State Chem.* **1999**, *145*, 541-548.

24. Bufaical, L.; Adriano, C.; Lora-Serrano, R.; Duque, J. G. S.; Mendonca-Ferreira, L.; Rojas-Ayala, C.; Baggio-Saitovitch, E.; Bittar, E. M.; Pagliuso, P. G., Structural, electronic and magnetic properties of the series of double perovskites $(Ca, Sr)_{(2-x)}La_xFeIrO_6$. *J. Solid State Chem.* **2014**, *212*, 23-29.

25. Bufaical, L.; Coutrim, L. T.; Santos, T. O.; Terashita, H.; Jesus, C. B. R.; Pagliuso, P. G.; Bittar, E. M., Physical properties of Sr_2FeIrO_6 and $Sr_{1.2}La_{0.8}FeIrO_6$ double perovskites obtained by a new synthesis route. *Materials Chemistry and Physics* **2016**, *182*, 459-465.

26. Kayser, P.; Alonso, J. A.; Mompean, F. J.; Retuerto, M.; Croft, M.; Ignatov, A.; Fernandez-Diaz, M. T., Crystal and Magnetic Structure of Sr_2BIrO_6 (B = Sc, Ti, Fe, Co, In) in the Framework of Multivalent Iridium Double Perovskites. *European Journal of Inorganic Chemistry* **2015**, 5027-5038.

27. Qasim, I.; Blanchard, P. E. R.; Liu, S.; Tang, C. G.; Kennedy, B. J.; Avdeev, M.; Kimpton, J. A., Ordered vs. disordered perovskites; structural studies of Fe-doped $SrIrO_3$ and $SrRuO_3$. *J. Solid State Chem.* **2013**, *206*, 242-250.

28. Larson, A. C.; Von Dreele, R. B. *General Structure Analysis System*, Los Alamos National Laboratory Report LAUR 86-748: 2000.

29. Lagarec, K.; G., R. D., Recaoil: Mössbauer spectral analysis software for windows. **1998**.

30. Anderson, M. T.; Greenwood, K. B.; Taylor, G. A.; Poeppelmeier, K. R., B-cation arrangements in double perovskites. *Prog. Solid St. Chem.* **1993**, *22*, 197.

31. King, G.; Woodward, P. M., Cation Ordering in Perovskites. *J. Mater. Chem.* **2010**, *20*, 5785-5796.

32. Pajskr, K.; Novak, P.; Pokorny, V.; Kolorenc, J.; Arita, R.; Kunes, J., On the possibility of excitonic magnetism in Ir double perovskites. *Phys. Rev. B* **2016**, *93*.

33. Kanungo, S.; Yan, B. H.; Felser, C.; Jansen, M., Active role of nonmagnetic cations in magnetic interactions for double-perovskite Sr_2BOsO_6(B = Y, In, Sc). *Phys. Rev. B* **2016**, *93*.

For Table of Contents Only. Sr_2FeIrO_6 adopts an $I\bar{1}$ distorted double perovskite structure. This distorted structure does not tolerate cation substitution, with low levels of A-site or Fe-site substitution leading to separation into two phases. In contrast to stoichiometric Sr_2FeIrO_6, cation substituted samples show evidence for an additional magnetic transition at $T_A \sim 220$ K, which indicates a $J_{eff} \neq 0$ behavior for the Ir^{5+} centers in the cation-substituted, $P2_1/n$ symmetry, double perovskite phases.

Sr_2FeIrO_6
$I\bar{1}$
$(a^-b^-c^-)$

cation
substitution

Sr_2FeIrO_6
$I\bar{1}$
$(a^-b^-c^-)$

+

$Sr_{2-x}A_xFeIrO_6$
$P2_1/n$
$(a^-a^-c^+)$